Optics Letters

Sub-150-fs pulses from an optically pumped broadband modelocked integrated external-cavity surface emitting laser

C. G. E. Alfieri,† D. Waldburger,† J. Nürnberg,* M. Golling, and U. Keller

Department of Physics, Institute for Quantum Electronics, ETH Zurich, Auguste-Piccard-Hof 1, 8093 Zurich, Switzerland
**Corresponding author: njacob@phys.ethz.ch*

Received 17 October 2018; revised 16 November 2018; accepted 19 November 2018; posted 19 November 2018 (Doc. ID 348499); published 17 December 2018

With a modelocked integrated external-cavity surface emitting laser (MIXSEL) we achieved a pulse duration of 144 fs. The MIXSEL belongs to the family of optically pumped semiconductor disk lasers. The MIXSEL operates at a center wavelength of 1033 nm with a 13-nm full width at half maximum optical bandwidth, at a pulse repetition rate of 2.73 GHz, and at an average output power of 30 mW. This new record result was obtained with an optimized multipair dielectric top-coating, a large bandgap $AlAs_xP_{1-x}$ material for strain compensation, a nonperiodic InGaAs quantum well gain structure, and an improved thermal management.

https://doi.org/10.1364/OL.44.000025

After a decade of constant and rapid development [1,2], ultrafast semiconductor disk lasers (SDLs) have achieved excellent performance for many application demonstrations such as dual comb spectroscopy [3], multiphoton microscopy [4], and frequency metrology [5,6]. Optically pumped vertical external cavity surface emitting lasers (VECSELs) [1] passively mode-locked with semiconductor saturable absorber mirrors (SESAMs) [7] have generated pulses as short as 100 fs [8] and several kilowatts of pulse peak power [9]. The mode-locked integrated external-cavity surface emitting laser (MIXSEL) [10] integrates the VECSEL gain and the SESAM saturable absorber into one wafer and therefore provides the most compact laser cavity and superior noise performance [11] comparable to ultrafast diode-pumped solid-state lasers. To date MIXSELs have demonstrated average output power up to 6.4 W [12], pulse repetition rates up to 100 GHz [13], and sub-200-fs pulses [14]. As an additional advantage, the semiconductor gain medium provides equal amplification for *s*- and *p*-polarized beams. In combination with the symmetry of the cavity geometry, the MIXSEL oscillator does not fix any preferred lasing polarization. A birefringent crystal inside the optical cavity can therefore separate the initially unpolarized beam in two cross-polarized pulse trains with slightly different pulse repetition rates sharing the same cavity [15], making the MIXSEL an ideal dual comb source.

After the first successful proof-of-principle demonstration of dual comb spectroscopy of water vapor performed with a free running picosecond MIXSEL emitting at 968 nm [3], a new generation of MIXSEL chips generating shorter pulses with a larger optical bandwidth and different emission wavelengths is very interesting for molecular spectroscopy [16–18] and for coherent supercontinuum generation [19].

In this Letter, we present a new milestone result for femtosecond MIXSELs. In contrast to previous sub-300-fs MIXSELs grown using both metal–organic vapor phase epitaxy (MOVPE) and molecular beam epitaxy (MBE) in a regrowth scheme [20], the new MIXSEL chip is grown on a single MBE machine to avoid the defects and the additional optical losses introduced by regrowth. The semiconductor structure is strain compensated, optimized for more efficient pump absorption and reduced two-photon absorption (TPA), and the thickness and position of the 11 quantum well (QW) gain layers are optimized for better pump absorption, lower gain saturation fluence, and a broader bandwidth. For dual comb mode-locking we also can demonstrate better uniformity and minimize thermal cross talk between the two beams on the chip.

We compared the thermal behavior of two 100-fs VECSEL chips. The chips consist of the same nominal epitaxial layer stack but are grown with MOVPE and MBE; the two VECSEL structures are described in detail in [8] and [5], respectively. From a thermal point of view, the VECSEL and MIXSEL chips show comparable thermal properties since they are both based on the same semiconductor $Al_xGa_{1-x}As$ material system with $In_xGa_{1-x}As$ QWs and P-containing layers for strain compensation. After substrate removal and flip-chip bonding on 5 mm × 5 mm, 1-mm-thick diamond substrates, we mount the samples on a copper heatsink. Through a Peltier element, we set the heatsink temperature to 10°C and optically pump the center of the chips with an 808-nm multimode laser diode. We shape the pump spot size to 400 μm diameter, set the absorbed pump power to ∼30 W, and observe the surface temperature profile with a thermal camera at a resolution of 25 μm, as depicted in Figs. 1(a) and 1(b). The pumped spots reach temperatures of ∼75°C for both samples. The MBE VECSEL shows a more efficient 1D heat flow resulting in a

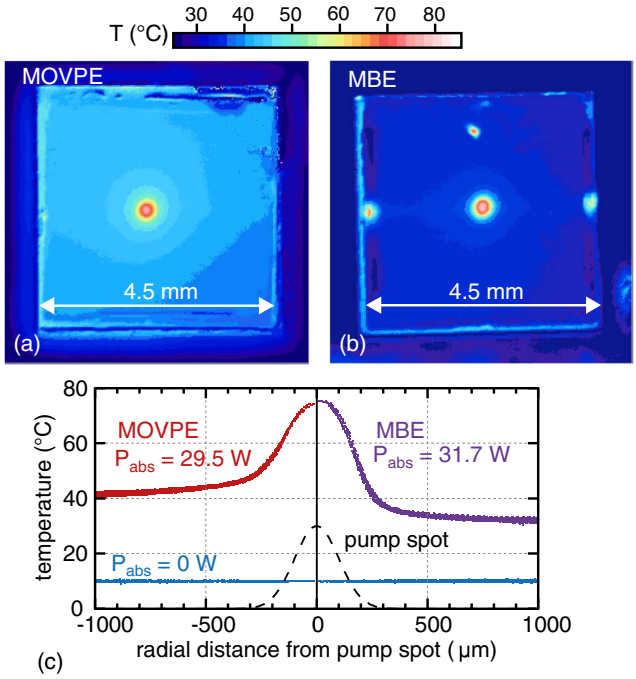

Fig. 1. Thermal image of optically pumped VECSEL chips grown with (a) MOVPE and (b) MBE. The MOVPE chip shows a pronounced lateral heat flow and a uniform heating of the entire surface. For the MBE chip the heated region is more restricted to the pumped area (hot points on the border are etch residuals). (c) Surface temperature as a function of the radial distance from the pumped spot. The MBE chip features an efficient 1D heat flow. At a distance of 300 µm from the center of the pump spot the surface temperature is ∼10°C lower compared to the MOVPE chip.

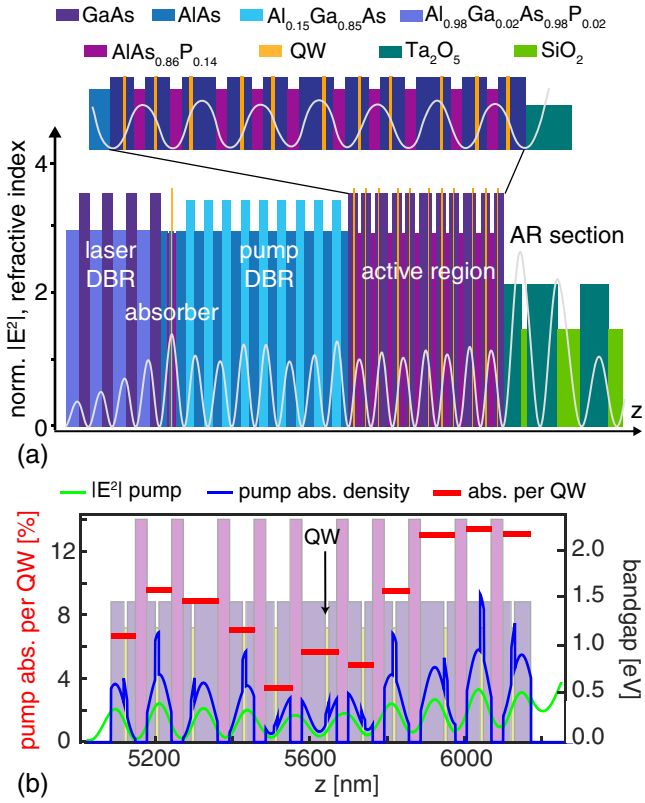

Fig. 2. (a) Layer stack of the semiconductor MIXSEL chip with zoom of the active region. The standing electric intensity wave is normalized to 4 outside of the reflective structure. The field intensity is enhanced at the absorber position to reduce its saturation fluence. (b) Pump absorption in the active region. The large-bandgap $AlAs_{0.86}P_{0.14}$ strain compensation layers do not absorb the pump light (abs. density = 0) and confine the optically generated carriers. The absorption of the standing pump wave for every QW reservoir (red bars) goes from a minimum of 3.3% more closer to a pump node to a maximum of 13%.

significantly decreased surface temperature at moderate distances from the pumped area.

Compared to the MOVPE chip, the surface temperature of the MBE VECSEL is ∼10°C lower at a 300-µm distance from the pump spot [Fig. 1(c)], which corresponds to the typical separation of the cross-polarized beams in dual comb operation [15]. Therefore, in our case the MBE structures clearly offer reduced undesired thermal effects such as overheated surface and thermal cross talk for dual comb mode-locking.

The epitaxial layer stack of the MIXSEL chip is depicted in Fig. 2(a). From bottom to top, the design features a 24-pair $GaAs/Al_{0.98}Ga_{0.02}As_{0.98}P_{0.02}$ distributed Bragg reflector (DBR) forming a high-reflectivity mirror with a stop band centered at the desired center lasing wavelength of 1033 nm. The small P-content provides a strain-free DBR, while 2% of Ga decreases oxidation in the thick Al layers for a longer chip lifetime. The absorber section is formed by a single 9-nm-thick $In_{0.23}Ga_{0.77}As$ QW embedded in AlAs and locally strain-compensated with 2 $AlAs_{0.86}P_{0.14}$ layers. A second 9.5-pair $Al_{0.15}Ga_{0.85}As/AlAs$ pump DBR avoids absorber bleaching from residual pump light at 808 nm. The following active region consists of 11 $In_{0.2}Ga_{0.8}As$ QWs embedded in GaAs. Most of strain-compensated SDLs operating at 1 µm usually use pump-absorbing tensile $GaAs_xP_{1-x}$ layers to balance the compressive strain introduced by the QWs [8,14,21]. However, here we use $AlAs_{0.86}P_{0.14}$ strain compensation layers. The large bandgap AlAsP-based materials are transparent for the pump beam and create a strong confinement for the carriers optically generated in the pump-absorbing GaAs barriers. This limits their diffusion and provides individual reservoirs of rapidly available carriers for each QW. In addition, large bandgap materials heavily reduce TPA in the active region, reducing the losses for short pulses [22]. The QWs are alternatively placed in slightly asymmetric pairs or singularly around the antinodes of the laser standing wave. The thickness and mutual position of QWs and strain-compensating and pump absorbing layers are optimized to simultaneously achieve perfect strain compensation, broadband operation, and sufficient absorption of the standing electric pump wave for every QW reservoir [>3%, Fig. 2(b)]. Additionally, the nonperiodic gain structure prevents subresonator effects due to the high refractive index contrast between the GaAs and the strain-compensating layers. The total pump absorption in the active region is maximized to ∼93%, and its reflection is minimized to ∼3% by a numerically optimized antireflection (AR) section consisting of 3 Ta_2O_5/SiO_2 pairs. The AR section is deposited with ion beam sputtering (IBS), which provides better thickness uniformity over the chip surface and higher film packing density [23,24] for more humidity-resistant layers compared to our plasma enhanced chemical vapor

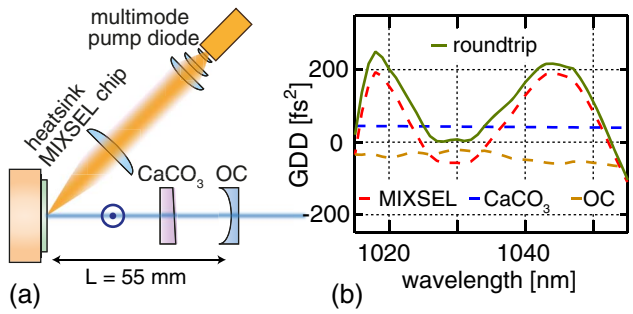

Fig. 3. (a) Straight linear MIXSEL cavity. The semiconductor MIXSEL chip forms one cavity end mirror and the OC the other. The intracavity calcite crystal fixes the laser polarization. The MIXSEL chip is pumped at 808 nm with a multimode diode laser array under a 45° angle. The total cavity length is set to 55 mm. (b) Dispersion profile of the cavity elements. The calcite crystal compensates the negative GDD of chip and OC at the designed lasing wavelength. The total cavity GDD is small and positive in the designed lasing spectral region.

deposition (PECVD). The entirely dielectric AR section further reduces additional TPA losses in the intense-field regions close to the chip surface and provides the desired flat ($< \pm 200$ fs^2) group delay dispersion (GDD) profile in a ±15 nm bandwidth around the center lasing wavelength. The DBRs, the GaAs barriers and the strain-compensating layers in the active region are grown at 580°C and the gain QWs at 510°C. The absorber QW is grown at 280°C to introduce defect recombination centers and assure the fast recovery dynamics indispensable for short pulse generation.

The structure is grown upside-down. After substrate removal through wet etching, the MIXSEL is flip-chip bonded on 1-mm-thick, 5 mm × 5 mm diamond heat sink and finally mounted on a Peltier-controlled, water-cooled copper substrate. The straight linear MIXSEL cavity is defined by two end mirrors with the MIXSEL chip at one side and a curved output coupler (OC) with a 100-mm radius of curvature and a 0.3% transmission at the other side [Fig. 3(a)]. We insert an intracavity AR coated 1-mm-thick wedged calcite ($CaCO_3$) birefringent crystal and align the cavity for the ordinary beam to select the lasing polarization. At 1033 nm, a 1-mm-thick calcite crystal introduces a GDD of 42 fs^2 in the *s*-polarized ordinary beam [Fig. 3(b)]. The wedged crystal (wedge angle 1°) allows for tuning the cavity roundtrip GDD to an ideally small positive and constant value (<50 fs^2) for ultrashort pulse generation [25] in the desired 1025–1035 nm lasing range [Fig. 3(b)]. Furthermore, the birefringent calcite crystal will support a second step to easily switch to dual comb mode-locking by pumping a second spot on the MIXSEL chip for the extraordinary beam.

For lasing operation, the chip temperature is stabilized to 4.5°C. Stable self-starting mode-locking is obtained at an incident pump power of 7.9 W and at a pulse repetition rate of 2.73 GHz. The relatively low average output power of 30 mW (compared to [20]) is a consequence of the broadband chip design. However, this power is sufficient for spectroscopy applications [26,27]. The optical-to-optical pump efficiency of <0.5% lies in the typical value range of sub-200-fs SDLs [2,14].

A thorough pulse characterization was carried out using a second harmonic generation frequency resolved optical gating (SHG FROG). The experimental and retrieved spectrograms depicted in Figs. 4(a)–4(b) show good agreement, with a FROG error <0.2% (matrix size: 512 × 512).

The retrieved temporal intensity reveals a pulse duration of 144 fs [Fig. 4(c)]. The small discrepancy with the 139-fs pulse duration indicated by the sech^2 fit of the SHG autocorrelation trace [Fig. 4(d)] is due to a not-perfect sech^2 shape of the mode-locked pulses. To date this is the shortest pulse achieved with the MIXSEL technology. The resulting pulse peak power is 70 W. The microwave spectrum confirms fundamental mode-locking with a narrow peak at the pulse repetition frequency

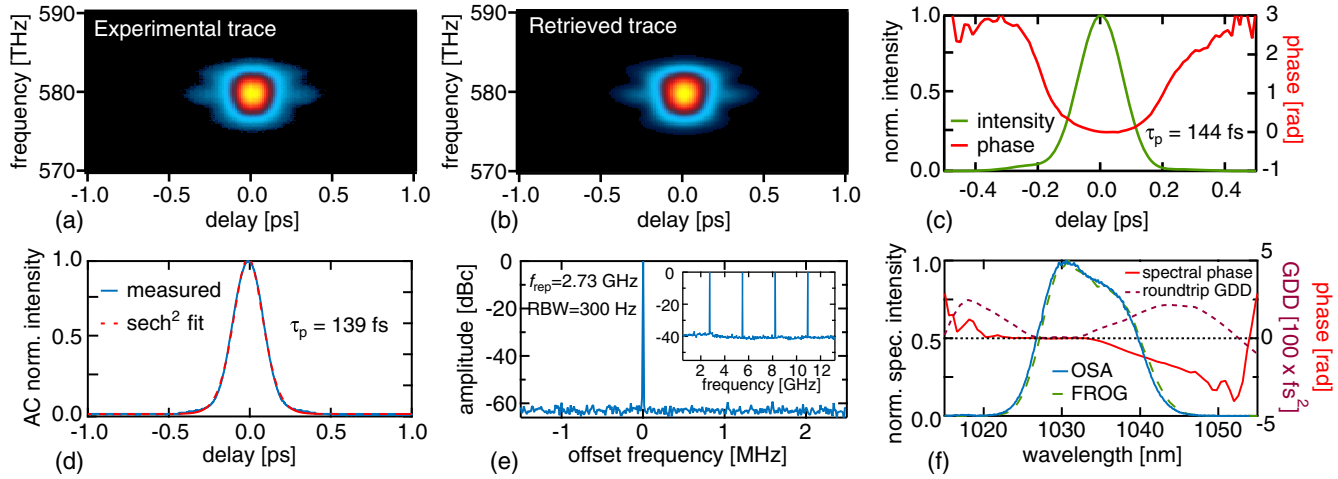

Fig. 4. Mode-locking diagnostics. (a) Measured and (b) retrieved FROG spectrograms. (c) Retrieved FROG temporal intensity, revealing a pulse duration of 144 fs and a flat temporal phase at the pulse center. (d) Autocorrelation trace; the sech^2 fit indicates a pulse duration of 139 fs. (e) Microwave spectrum with high signal to noise ratio >60 dB for the peak corresponding to the pulse repetition rate of 2.73 GHz. Inset: large span of the microwave spectrum; all the higher harmonics of the pulse repetition rate are present with equal spectral power. (f) Optical spectrum; the retrieved FROG trace and the one taken with the optical spectrum analyzer overlap. The spectral phase is relatively flat but indicates a chirp in the tail of the spectrum, spectrally corresponding to where the roundtrip GDD significantly deviates from zero.

and more than 60 dB of signal to noise ratio [Fig. 4(e)]. All the higher harmonics of the fundamental pulse repetition rate appear with equal power in the long-span measurement of the microwave spectrum [Fig. 4(e), inset]. SHG FROG and an optical spectrum analyzer confirm that the optical spectrum is centered at 1033 nm with a 13-nm full width at half maximum (FWHM) bandwidth [Fig. 4(f)]. Such bandwidth could support sub-100-fs transform-limited pulses, but the imperfectly flat retrieved spectral phase indicates a chirp of the high-wavelength tail of the spectrum, where the round-trip GDD significantly deviates from the optimum small positive value. To highlight the enhanced spectroscopic potential of this structure, we underline that the large spectral width achieved here is >70% wider compared to the previous record MIXSEL described in [14] and 40 times wider than in the first proof-of-principle dual comb experiment [3].

To conclude, we presented a significant advance in ultrashort pulse generation with MIXSELs. We implemented high bandgap strain-compensating layers to reduce TPA losses for short pulses with high peak powers and obtain higher carrier confinement in the gain regions. Finally, we deposited a fully dielectric AR section with IBS, which offers better material homogeneity than PECVD. With this chip, the MIXSEL technology demonstrated pulses as short as 144 fs with a 13-nm FWHM optical bandwidth. This was possible thanks to the broadband gain of the semiconductor structure and to the accurate optimization of the GDD profile for each cavity element. This MIXSEL chip has been used for femtosecond dual comb spectroscopy demonstration where we measured acetylene gas transmittance with a resolution of 2.7 GHz without aliasing effects in 100 ms with residual errors of less than 3% [16–18].

Funding. D-A-CH program with the QD-MIXSEL project, which was scientifically evaluated by the Swiss National Science Foundation (SNSF); Deutsche Physikalische Gesellschaft (DPG) (ETH-49 18-1).

Acknowledgment. The authors acknowledge support of the technology and cleanroom facility FIRST of ETH Zürich for advanced micro- and nanotechnology. The authors thank Dr. Valentin Wittwer from the University of Neuchâtel for technical help and IBS depositions.

†These authors contributed equally to this work.

REFERENCES

1. M. Guina, A. Rantamäki, and A. Härkönen, J. Phys. D: Appl. Phys. **50**, 383001 (2017).
2. B. W. Tilma, M. Mangold, C. A. Zaugg, S. M. Link, D. Waldburger, A. Klenner, A. S. Mayer, E. Gini, M. Golling, and U. Keller, Light: Sci. Appl. **4**, e30 (2015).
3. S. M. Link, D. J. H. C. Maas, D. Waldburger, and U. Keller, Science **356**, 1164 (2017).
4. F. F. Voigt, F. Emaury, P. Bethge, D. Waldburger, S. M. Link, S. Carta, A. V. D. Bourg, F. Helmchen, and U. Keller, Biomed. Opt. Express **8**, 3213 (2017).
5. D. Waldburger, A. S. Mayer, C. G. E. Alfieri, A. R. Johnson, X. Ji, A. Klenner, Y. Okawachi, M. Lipson, A. L. Gaeta, and U. Keller, *Laser Congress 2017 (ASSL, LAC)* (Optical Society of America, 2017), p. ATu6A.3.
6. N. Jornod, K. Gürel, V. J. Wittwer, P. Brochard, S. Hakobyan, S. Schilt, D. Waldburger, U. Keller, and T. Südmeyer, Optica **4**, 1482 (2017).
7. U. Keller, K. J. Weingarten, F. X. Kärtner, D. Kopf, B. Braun, I. D. Jung, R. Fluck, C. Hönninger, N. Matuschek, and J. Aus der Au, IEEE J. Sel. Top. Quantum Electron. **2**, 435 (1996).
8. D. Waldburger, S. M. Link, M. Mangold, C. G. E. Alfieri, E. Gini, M. Golling, B. W. Tilma, and U. Keller, Optica **3**, 844 (2016).
9. C. W. Baker, M. Scheller, A. Laurain, A. Ruiz-Perez, W. Stolz, S. Addamane, G. Balakrishnan, S. W. Koch, R. J. Jones, and J. V. Moloney, IEEE Photon. Technol. Lett. **29**, 326 (2017).
10. D. J. H. C. Maas, A.-R. Bellancourt, B. Rudin, M. Golling, H. J. Unold, T. Südmeyer, and U. Keller, Appl. Phys. B **88**, 493 (2007).
11. M. Mangold, S. M. Link, A. Klenner, C. A. Zaugg, M. Golling, B. W. Tilma, and U. Keller, IEEE Photon. J. **6**, 1 (2014).
12. B. Rudin, V. J. Wittwer, D. J. H. C. Maas, M. Hoffmann, O. D. Sieber, Y. Barbarin, M. Golling, T. Südmeyer, and U. Keller, Opt. Express **18**, 27582 (2010).
13. M. Mangold, C. A. Zaugg, S. M. Link, M. Golling, B. W. Tilma, and U. Keller, Opt. Express **22**, 6099 (2014).
14. C. G. E. Alfieri, D. Waldburger, S. M. Link, E. Gini, M. Golling, G. Eisenstein, and U. Keller, Opt. Express **25**, 6402 (2017).
15. S. M. Link, A. Klenner, M. Mangold, C. A. Zaugg, M. Golling, B. W. Tilma, and U. Keller, Opt. Express **23**, 5521 (2015).
16. J. Nürnberg, C. G. E. Alfieri, Z. Chen, D. Waldburger, N. Picqué, and U. Keller, "An unstabilized femtosecond semiconductor laser for dual-comb spectroscopy of acetylene," submitted to Opt. Express.
17. J. Nürnberg, C. G. E. Alfieri, Z. Chen, D. Waldburger, M. Golling, N. Picqué, and U. Keller, *CLEO: Science and Innovations*, San Jose, California (Optical Society of America, 2018), p. JW2A.157.
18. J. Nürnberg, C. G. E. Alfieri, Z. Chen, D. Waldburger, M. Golling, N. Picqué, and U. Keller, *Advanced Photonics Congress*, Zurich, Switzerland (Optical Society of America, 2018), p. IM3I.1.
19. D. Waldburger, A. S. Mayer, C. G. E. Alfieri, J. Nürnberg, A. R. Johnson, X. Ji, A. Klenner, Y. Okawachi, M. Lipson, A. L. Gaeta, and U. Keller, "Tightly locked optical frequency comb from a semiconductor disk laser," submitted to Optica.
20. M. Mangold, M. Golling, E. Gini, B. W. Tilma, and U. Keller, Opt. Express **23**, 22043 (2015).
21. A. Laurain, R. Rockmore, H.-T. Chan, J. Hader, S. W. Koch, A. R. Perez, W. Stolz, and J. V. Moloney, J. Opt. Soc. Am. B **34**, 329 (2017).
22. C. G. E. Alfieri, A. Diebold, F. Emaury, E. Gini, C. J. Saraceno, and U. Keller, Opt. Express **24**, 27587 (2016).
23. J. E. Klemberg-Sapieha, J. Oberste-Berghaus, L. Martinu, R. Blacker, I. Stevenson, G. Sadkhin, D. Morton, S. McEldowney, R. Klinger, P. J. Martin, N. Court, S. Dligatch, M. Gross, and R. P. Netterfield, Appl. Opt. **43**, 2670 (2004).
24. E. Çetinörgü, B. Baloukas, O. Zabeida, J. E. Klemberg-Sapieha, and L. Martinu, Appl. Opt. **48**, 4536 (2009).
25. O. D. Sieber, M. Hoffmann, V. J. Wittwer, M. Mangold, M. Golling, B. W. Tilma, T. Südmeyer, and U. Keller, Appl. Phys. B **113**, 133 (2013).
26. T. Ideguchi, A. Poisson, G. Guelachvili, N. Picque, and T. W. Hänsch, Nat. Commun. **5**, 3375 (2014).
27. X. Zhao, G. Hu, B. Zhao, C. Li, Y. Pan, Y. Liu, T. Yasui, and Z. Zheng, Opt. Express **24**, 21833 (2016).